

Predicted stable two-dimensional semiconductor TiOS materials with promising photocatalytic properties: First-principles calculations

Pan Zhang(张攀), Shihai Fu(付世海), Chunying Pu(濮春英), Xin Tang(唐鑫), and Dawei Zhou(周大伟)

Citation : Chin. Phys. B, 2025, 34 (**5**): 057103. DOI: 10.1088/1674-1056/adb687
http://cpb.iphy.ac.cn; http://iopscience.iop.org/cpb

What follows is a list of articles you may be interested in

Multi-objective global optimization approach predicted quasi-layered ternary TiOS crystals with promising photocatalytic properties

Yi-Jie Xiang(向依婕), Siyan Gao(高思妍), Chunlei Wang(王春雷), Haiping Fang(方海平), Xiangmei Duan(段香梅), Yi-Feng Zheng(郑益峰), and Yue-Yu Zhang(张越宇)
Chin. Phys. B, 2024, 33 (**8**): 087101. DOI: 10.1088/1674-1056/ad4bc3

Two-dimensional CrP_2 with high specific capacity and fast charge rate for lithium-ion battery

Xiaoyun Wang(王晓允), Tao Jing(荆涛), and Dongmei Liang(梁冬梅)
Chin. Phys. B, 2023, 32 (**6**): 067102. DOI: 10.1088/1674-1056/acc5e0

Modulation of Schottky barrier in XSi$_2$N$_4$/graphene (X=Mo and W) heterojunctions by biaxial strain

Qian Liang(梁前), Xiang-Yan Luo(罗祥燕), Yi-Xin Wang(王熠欣), Yong-Chao Liang(梁永超), and Quan Xie(谢泉)
Chin. Phys. B, 2022, 31 (**8**): 087101. DOI: 10.1088/1674-1056/ac5c3b

Stability, electronic structure, and optical properties of lead-free perovskite monolayer $Cs_3B_2X_9$ (B=Sb, Bi; X=Cl, Br, I) and bilayer vertical heterostructure $Cs_3B_2X_9$/$Cs_3B_2'X_9$ (B,B'=Sb, Bi; X=Cl, Br, I)

Yaowen Long(龙耀文), Hong Zhang(张红), and Xinlu Cheng(程新路)
Chin. Phys. B, 2022, 31 (**2**): 027102. DOI: 10.1088/1674-1056/ac2e5f

Structure prediction, electronic, and mechanical properties of alkali metal MB_{12} (M= Be, Mg, Ca, Sr) from first principles

Chun-Ying Pu(濮春英), Rong-Mei Yu(于荣梅), Ting Wang(王婷), Zhen-Yan X\"ue(薛振彦), Yong-Sheng Zhu(朱永胜), and Da-Wei Zhou(周大伟)
Chin. Phys. B, 2021, 30 (**1**): 017102. DOI: 10.1088/1674-1056/abb667

Predicted stable two-dimensional semiconductor TiOS materials with promising photocatalytic properties: First-principles calculations

Pan Zhang(张攀)[1], Shihai Fu(付世海)[1], Chunying Pu(濮春英)[1], Xin Tang(唐鑫)[2], and Dawei Zhou(周大伟)[1,†]

[1] *College of Physics and Electronic Engineering, Nanyang Normal University, Nanyang* 473061, *China*
[2] *College of Material Science and Engineering, Guilin University of Technology, Guilin* 541004, *China*

(Received 26 November 2024; revised manuscript received 30 January 2025; accepted manuscript online 17 February 2025)

TiO_2 is a well-known photocatalyst with a band gap of 3.2 eV, yet its ability to absorb light is limited to the short wavelengths of ultraviolet light. To achieve a more effective photocatalytic material, we have designed two-dimensional semiconductor TiOS materials using swarm intelligence algorithms combined with first-principles calculations. Three stable low-energy structures with space groups of $P2_1/m$, $P3m1$ and $P2_1/c$ are identified. Among these structures, the Janus $P3m1$ phase is a direct bandgap semiconductor, while the $P2_1/m$ and $P2_1/c$ phases are indirect bandgap semiconductors. Utilizing the accurate hybrid density functional HSE06 method, the band gaps of the three structures are calculated to be 2.34 eV ($P2_1/m$), 2.24 eV ($P3m1$) and 3.22 eV ($P2_1/c$). Optical calculations reveal that TiOS materials exhibit a good light-harvesting capability in both visible and ultraviolet spectral ranges. Moreover, the photocatalytic calculations also indicate that both $P2_1/m$ and $P3m1$ TiOS can provide a strong driving force for converting H_2O to H_2 and O_2 in an acidic environment with pH = 0. The structural stabilities, mechanical properties, electronic structures and hydrogen evolution reaction activities are also discussed in detail. Our research suggests that two-dimensional TiOS materials have potential applications in both semiconductor devices and photocatalysis.

Keywords: first principles, structure prediction, TiOS semiconductor, photocatalysis

PACS: 71.15.Mb, 61.46.–w, 71.15.Nc

DOI: 10.1088/1674-1056/adb687 **CSTR:** 32038.14.CPB.adb687

1. Introduction

The scarcity of energy, the consumption of fossil fuels and the pollution they cause have created an urgent need to find cleaner sources of energy. Among the many renewable energy sources, light energy is one of the most sustainable and clean energy sources on Earth, and is closely related to our daily lives. The efficient and rational use of light energy is crucial for the future of human life.[1] The advent of photocatalysis has led to the application of light energy and its conversion into other forms of energy that can be harvested and utilized. Polycrystalline TiO_2 is an important functional material due to its better stability, ease of preparation, non-toxicity, low cost and high photocatalytic activity, and has potential applications in many fields [2–5] such as medicine,[6] optoelectronic devices[7] and particularly in the field of photocatalysis. In fact, TiO_2 has been one of the most widely studied photocatalysts since its photocatalytic activity was first reported by Fujishima and Honda in 1972.[8]

However, TiO_2 has a band gap of 3.2 eV[9] and can only absorb short wavelengths of ultraviolet (UV) light, which makes up a very small fraction of the solar spectrum. As a result, TiO_2 has a very low utilization of light energy, leading to low photocatalytic efficiency.[10,11] This drawback significantly limits the widespread application of TiO_2 as a photocatalytic material. To enhance the absorption of solar energy in the visible light spectrum, various modifications have been utilized for TiO_2, among which doping has proven to be highly effective.[12–16] By adding doping impurity elements, impurity energy levels can be formed within the band gap of TiO_2, resulting in visible-light-responsive photocatalytic activity and increased stability when exposed to UV radiation.[17] Previous studies have shown that non-metallic doping is more effective than metallic doping, such as the introduction of N,[18] S[19] and C[20] into TiO_2.[21] In particular, S doping has shown some advantages.[22,23] S doping can tune the position of the valence band maximum (VBM) while leaving the conduction band minimum (CBM) unchanged. Theoretically, Cui *et al.*[23] reported that S-doped TiO_2 successfully narrows the band gap due to the presence of an isolated S 3p state at the upper edge of the VBM. Experimental studies have also shown the advantages of S doping. For example, S-doped TiO_2 was reported to lead to a significant shift of the absorption edge towards the low-energy region.[24] Higher doping concentrations of S using various methods[25–33] have been employed to further enhance visible optical absorption and photocatalytic properties. Therefore, in recent studies more attention has been paid to high concentrations of S doping into TiO_2. Jovanovic *et al.* utilized an *ab initio* method to examine the crystal structures of TiO_2–S solid solutions, investigating the pressure-induced phase transitions in these compounds.[34] Very recently, using

†Corresponding author. E-mail: zhoudawei@nynu.edu.cn

© 2025 Chinese Physical Society and IOP Publishing Ltd. All rights, including for text and data mining, AI training, and similar technologies, are reserved.

multi-objective global optimization, Xiang *et al.*[35] proposed two quasi-layered ternary Ti–O–S crystals that hold the potential for achieving high-efficiency photochemical conversion.

In this work, we focus on two-dimensional (2D) TiOS materials, and investigate their potential as photocatalytic materials. As is well known, 2D materials have advantages as photocatalysts over their bulk counterparts. For example, 2D materials have a higher specific surface area, more reaction sites, excellent light absorption ability and better charge separation and transmission properties. In addition, 2D materials generally have a different bandgap from their bulk counterparts, which provides the possibility for 2D TiOS materials to be a good photocatalytic material. We notice that Barhoumi *et al.* recently proposed a bulk TiOS material together with its 2D monolayer. They found that the bulk TiOS is metallic, whereas the corresponding 2D TiOS has a large band gap of ~ 4.5 eV.[36]

However, the 2D TiOS proposed by Barhoumi *et al.* may not be energetically stable 2D TiOS materials. To explore the ground state structures, the particle swarm optimization (PSO) method through global structure prediction and first-principles calculations, implemented in the CALYPSO code,[37] has been shown to be an effective tool. This method has been successful in predicting various low-dimensional materials. Therefore, in this work we systematically explored the stable 2D TiOS structures using the CALYPSO code and identified three new stable 2D TiOS structures. The structural stability and mechanical, electronic, optical and photocatalytic properties of the TiOS materials were systematically investigated by first-principles calculations. Along with the discovery of new 2D TiOS materials, we found TiOS to be potential semiconductor-device and photocatalytic materials.

2. Computational method

The 2D TiOS structures were explored using the CALYPSO program based on the PSO algorithm in combination with first-principles calculations using molecular formulae from one- to four-fold. To allow the structures to converge, 40 structures were generated per generation and a total of 40 generations were set up until the calculation was stopped by 16 consecutive occurrences of structures with lower energies. A vacuum distance of 25.0 Å was set in the z-axis to avoid the influence of weak van der Waals forces between the layers. All calculations in this paper were based on VASP software,[38–40] and the exchange–correlation energy was estimated using the generalized gradient approximation (GGA)[41] with the Perdew–Burke–Ernzerhof (PBE) functional.[42] To get a convergence result, the plane wave cutoff energy was set to 520 eV, while the k-point mesh[43] was set to $10\times6\times1$ for $P2_1/m$ and $12\times12\times1$ and $5\times6\times1$ for $P3m1$ and $P2_1/c$, respectively. The self-consistent field was calculated so that the energy converged to within 1×10^{-6} eV/atom and the atomic force did not exceed 0.01 eV/atom. To avoid the problem of underestimated energy gaps caused by the PBE functional, the Heyd–Scuseria–Ernzerhof (HSE06)[44,45] method was chosen to calculate the energy band structures of the materials. In addition, the finite displacement approach as implemented in the Phonopy package[46] was chosen to calculate the phonon spectra. Molecular dynamics simulations (AIMD) were performed using the NVT canonical criterion for $2\times2\times1$ ($P2_1/m$ and $P3m1$) and $4\times4\times1$ ($P2_1/c$) supercell structures. The Gibbs free energy of H* (ΔG_{H^*}) was calculated according to the following equation:

$$\Delta G_{M^*} = \Delta E_{M^*} + \Delta E_{\mathrm{ZPE}} - T\Delta S, \tag{1}$$

where ΔE_{M^*} denotes the adsorption energy of the intermediate M^* adsorbed on the surface and ΔE_{ZPE} is the difference in the zero-point energy between the adsorbed state and the gas phase state; the third term $T\Delta S$ is the contribution of the entropy difference between the adsorbed hydrogen and hydrogen in the gas phase. During the hydrogen evolution reaction (HER) calculations, a GGA+U method[47] with a U value of 3 eV for Ti was used. To investigate the chemical reactivity of $P2_1/m$ and $P3m1$ TiOS, three different adsorption sites were considered in order to determine the adsorption energies of the intermediates on the 2D TiOS materials: (1) on top of the O atom in a $3\times3\times1$ supercell, (2) on top of the S atom, (3) in the center of the surface hexagon. It was found that hydrogen adsorption is most favorable at the top of the S atom.

3. Results and discussion

3.1. Crystal structure

Using the structure search method as implemented in the CALYPSO program, three lower-energy 2D TiOS structures with space groups $P2_1/m$, $P3m1$ and $P2_1/c$ were obtained. Top and side views of the $P2_1/m$ TiOS are shown in Fig. 1(a), with O and S atoms alternating on either side of the Ti atom, similar to the 1T structure of transition metal disulfides. However, for the $P3m1$ phase, as seen in Fig. 1(b), O and S atoms are found separately on each side of the Ti atom layer. The $P3m1$ phase is the so-called 2D Janus phase. In 2D Janus structures, one type of atom in a layer is completely substituted with another type of atom of the same group, breaking the out-of-plane symmetry. 2D Janus materials do not exist in nature,[48] but have been synthesized experimentally by means of the selective epitaxial atomic replacement (SEAR) method. Using this method, researchers have successfully synthesized a number of 2D Janus transition metal dichalcogenides including MoSSe,[49,50] WSSe[49,51] and PtSSe.[52] These asymmetric Janus structures exhibit distinct physical and chemical

properties, including excellent catalytic, piezoelectric, thermoelectric, magnetic and valley polarization properties.[53–58] Therefore the Janus $P3m1$ phase may also exhibit excellent physical and chemical properties. More interestingly, we note that the predicted 2D $P2_1/m$ and $P3m1$ TiOS can be seen as isolated single monolayers of the Ti–O–S bulk materials proposed by Xiang *et al.*[35] Hence, these two phases may be synthesized from TiOS bulk materials using a simple exfoliation method instead of the SEAR method. Figure 1(c) shows the structure of the $P2_1/c$ phase, which contains four Ti, four O and four S. For the $P2_1/c$ phase, the O and S atoms show a mixed arrangement on the upper and lower surfaces of the Ti atomic layer. Thus, the main difference between the three predicted TiOS materials is the different arrangement of O and S atoms, i.e., spaced arrangement, top–bottom arrangement and mixed arrangement.

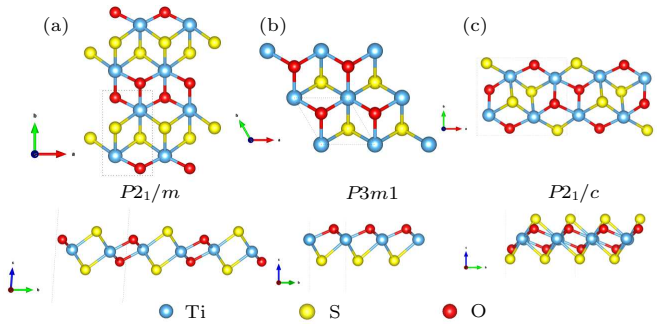


Fig. 1. Top and side views of the three structures of 2D TiOS: (a) $P2_1/m$, (b) $P3m1$ and (c) $P2_1/c$. Ti, S and O atoms are represented by blue, yellow and red spheres, respectively.

To clarify the thermal stability of the 2D TiOS, the cohesive energy was calculated and defined as $E_{\text{coh}} = (mE_{\text{Ti}} + mE_{\text{O}} + mE_{\text{S}} - E_{\text{TiOS}})/3m$, where E_{Ti}, E_{O} and E_{S} are the total energies of an isolated Ti atom, an isolated O atom and an isolated S atom, respectively, E_{TiOS} is the total energy of the TiOS unit cell, and m is the number of Ti, O and S atoms in the TiOS compound. The cohesive energies, lattice parameters, bond lengths between the nearest atoms and bond angles in the three predicted phase structures as well as the already known $P4/nmm$ structure proposed by Barhoumi *et al.* are given in Table 1.[36] The cohesive energies of these three structures are higher than that of the $P4/nmm$ structure, which implies that the three structures are more stable energetically. Furthermore, the cohesive energies of the predicted phases exceed those of other common 2D materials such as MoS_2 (4.97 eV/atom),[59] silicene (3.98 eV/atom), germanene (3.26 eV/atom)[60] and phosphorene (3.61 eV/atom),[61,62] demonstrating the thermodynamic stability of the predicted phases. To further investigate the chemical bonding, the charge density difference was calculated and is shown in Fig. 2. Charge density difference is defined as the total electron density of the TiOS minus the electron density of isolated Ti, O and S atoms at their respective positions. It is evident that the electrons are localized around the O atoms and show ionic bonding character between Ti and O. Bader charge analysis[63] shows that each O atom in $P2_1/m$, $P3m1$ and $P2_1/c$ accepts a net electronic charge of $1.09e$, $1.03e$ and $0.98e$, respectively, from the Ti atom. It is also notable from Fig. 2 that there is a clear charge localization between Ti and S, indicating that the Ti–S bond is mainly a covalent bond.

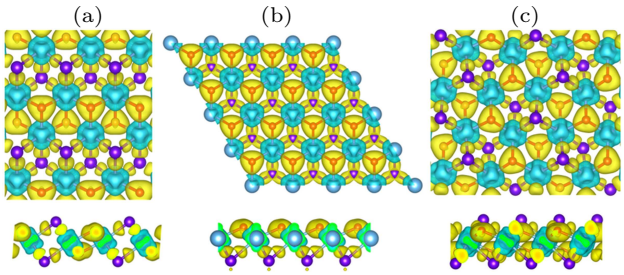


Fig. 2. Charge density difference of the TiOS for (a) the $P2_1/m$ structure, (b) the $P3m1$ structure and (c) the $P2_1/c$ structure. Gold indicates a charge increase and cyan indicates charge depletion. The isosurface value is set 0.01 $e{\cdot}\text{Å}^{-3}$. The blue atoms are Ti atoms, the purple atoms are S atoms and the red atoms are O atoms.

Table 1. Calculated cohesive energy, bond lengths, bond angles and lattice constants (a and b) for the TiOS materials.

Phase	Cohesive energy (eV)	Ti–S (Å)	Ti–O (Å)	S–Ti–O (°)	O–Ti–O (°)	a (Å)	b (Å)
$P2_1/m$	7.841	2.474	1.942	83.23	80.88	3.214	5.520
$P3m1$	7.811	2.425	1.995	85.30	105.02	3.166	2.741
$P2_1/c$	7.841	2.503	1.949	85.47	79.12	6.393	5.488
$P4/nmm$	7.742	2.638	2.023	77.99	69.43	3.258	3.259

3.2. Structure stability

In addition to the thermal stability, we further checked the dynamical stabilities using the phonon dispersion curves. Figure 3 shows the calculated phonon spectra of the 2D TiOS materials. There are small imaginary frequencies around the Gamma point, which are typically associated with the 2D nature of these materials or the lack of translational symmetry in the Phononpy program. Apart from minor errors around the Gamma points, there are no negative frequencies in the entire Brillouin zone. indicating that they are dynamically stable. We also performed molecular dynamic simulations to test the stability of 2D TiOS materials at finite temperature. The simulated temperature was set to 300 K, the time step was 2 fs; the results are shown in Fig. 4. The calculations show that the total energy of the TiOS materials oscillates around a stable value as a function of time. After 40 ps, the 2D crystal structures

retain good integrity. The TiOS supercells show no obvious atomic rearrangement or bond breaking throughout the process. Therefore, we can conclude that the TiOS materials have good stability at room temperature.

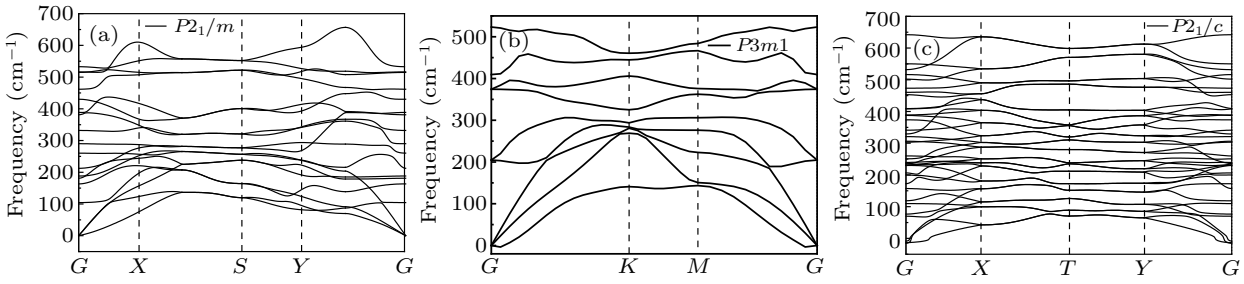


Fig. 3. Phonon spectra of 2D TiOS materials for (a) the $P2_1/m$ structure, (b) the $P3m1$ structure and (c) the $P2_1/c$ structure.

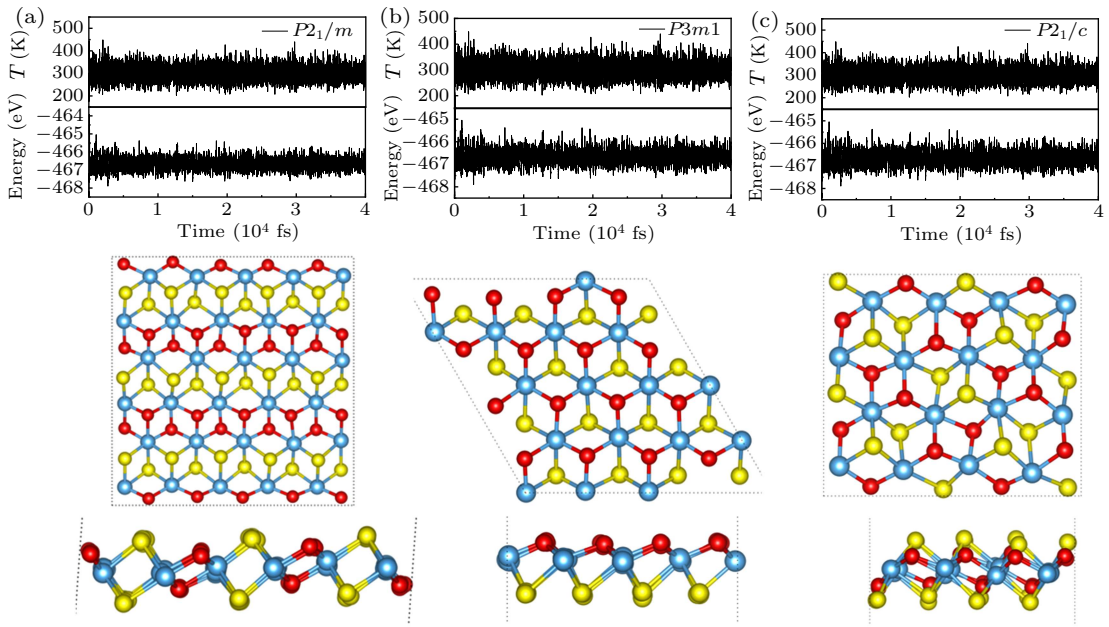


Fig. 4. Molecular dynamics simulation of the 2D TiOS structures: (a) $P2_1/m$ structure, (b) $P3m1$ structure, (c) $P2_1/c$ structure.

3.3. Mechanical properties

Elastic constants are physical quantities that describe the elastic behavior of a solid material and characterize the response of a material when it is subjected to a force or deformation. They can also be used to check the mechanical stability of a crystal. The calculated elastic constants of the predicted TiOS structures are listed in Table 2. If a structure is stable it is required that its elastic constant matrix must be positive definite. It is evident that all the elastic constants satisfy the necessary mechanical equilibrium conditions,[64] confirming the mechanical stability of 2D TiOS materials.

Table 2. Calculated elastic constants of the predicted 2D TiOS.

Structure	C_{11} (GPa)	C_{22} (GPa)	C_{12} (GPa)	C_{66} (GPa)
$P2_1/m$	106.83	98.0	24.34	39.57
$P3m1$	124.53	–	34.39	45.06
$P2_1/c$	99.94	111.03	31.64	43.18

Moreover, the orientation angle (θ) dependent Young's modulus $E(\theta)$, Poisson's ratio $v(\theta)$ and shear modulus $G(\theta)$ (i.e., the angle with respect to the x-axis) in the x–y plane were also calculated from the elastic constants of the 2D TiOS. The formulae used were as follows:[65]

$$E(\theta)=\frac{C_{11}C_{12}-C_{12}^2}{C_{11}\sin^4\theta+\left(\frac{C_{11}C_{12}-C_{12}^2}{C_{66}}-2C_{12}\right)\sin^2\theta\cos^2\theta+C_{22}\cos^4\theta}, \quad (2)$$

$$v(\theta)=\frac{C_{12}\sin^4\theta-\left(C_{11}+C_{12}-\frac{C_{11}C_{12}-C_{12}^2}{C_{66}}\right)\sin^2\theta\cos^2\theta+C_{12}\cos^4\theta}{C_{11}\sin^4\theta+\left(\frac{C_{11}C_{12}-C_{12}^2}{C_{66}}-2C_{12}\right)\sin^2\theta\cos^2\theta+C_{22}\cos^4\theta}, \quad (3)$$

$$G(\theta)=E(\theta)/(2\cdot(1+v(\theta))). \quad (4)$$

The results for the mechanical properties are shown in Fig. 5. Due to the spatial inversion symmetry, the elastic properties of the $P3m1$ structure (including Young's modulus, Poisson's ratio and shear modulus) exhibit isotropy, with values of 115.0 GPa for Young's modulus, 45.06 GPa for shear modulus

and 0.276 for Poisson's ratio. In contrast, the elastic properties of the $P2_1/m$ and $P2_1/c$ structures are more anisotropic. As seen in Fig. 5(c), the Poisson's ratio for the $P2_1/m$ structure forms an elliptical shape, indicating that the material is nearly isotropic, with minimal variation in elasticity across different directions. The maximum value is 0.248 along the x-axis, and the minimum is 0.227 in the 90° direction. For the $P2_1/c$ structure, the Poisson's ratio fluctuates more significantly, reaching a maximum of 0.317 in the 90° direction and a minimum of 0.225 in the 135° direction.

The shear modulus of the $P2_1/m$ structure in Fig. 5(b) has a narrow range of variation between 38.96 GPa and 39.57 GPa, while the shear modulus of the $P2_1/c$ structure shows a wider range from 36.81 GPa to 43.18 GPa. In Fig. 5(a), both $P2_1/m$ and $P2_1/c$ exhibit noticeable changes in Young's modulus, ranging from 92.4 GPa to 100.8 GPa for $P2_1/m$ and 90.9 GPa to 106.7 GPa for $P2_1/c$. For the Young's modulus, it is clear that the value for $P2_1/c$ TiOS falls between 80 GPa and 120 GPa, as shown in Fig. 5(a). Compared with some typical 2D materials, its Young's modulus is much lower than that of graphene (1 TPa) and graphene oxide (200 GPa)[66] but higher than that of black phosphorus (41.3 GPa).[67] TiOS has a higher Poisson's ratio than graphene (0.175),[68] with a maximum of 0.35 and a minimum of 0.2. This makes 2D TiOS a material with a positive Poisson's ratio and a moderately low Young's modulus, suggesting its potential for use in flexible electronic materials.

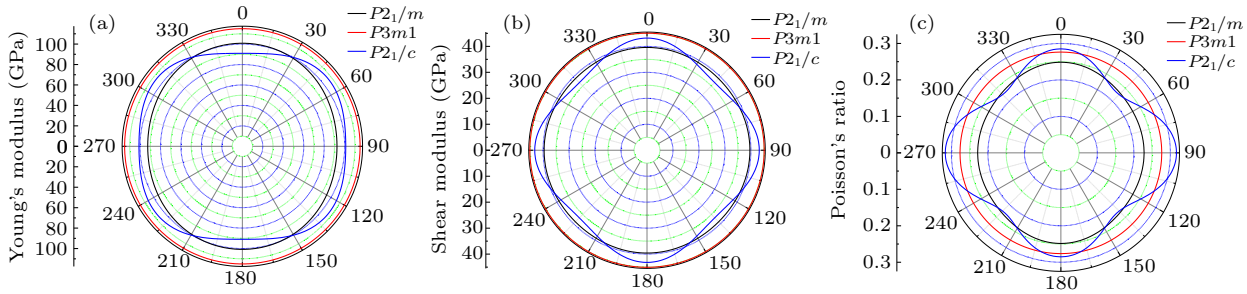


Fig. 5. The orientation angle (θ) dependent (a) Young's modulus $E(\theta)$, (b) shear modulus $G(\theta)$ and (c) Poisson's ratio $v(\theta)$ of the TiOS materials (x is the horizontal direction).

3.4. Electronic structure

We know that first-principles calculations using the PBE functional usually underestimate the bandgaps of materials, so we calculated the bandgaps of the TiOS structures using the HSE functional together with the PBE functional. The results of these calculations are shown in Fig. 6. Energy bands and densities of states show that the valence band peaks are mainly contributed by S atoms and the conduction band is mainly contributed by Ti atoms. Using the PBE approach, the band gaps of the $P2_1/m$, $P3m1$ and $P2_1/c$ structures were estimated to be 0.66 eV, 0.57 eV and 1.41 eV, respectively. The results obtained using the HSE functional are shown by the purple lines in Fig. 6. The calculated band gaps of $P2_1/m$, $P3m1$ and $P2_1/c$ structures are 2.34 eV, 2.23 eV and 3.22 eV, respectively. The band gaps of the $P3m1$ and $P2_1/c$ structures of TiOS are smaller than those of the $P4/nmm$ structure proposed by Barhoumi *et al.*[36] In previous work, the band gap of 2D TiO_2 with the $P6m2$ phase was reported to be 2.76 eV, while the band gap of the known 1T structure of TiO_2 was reported to be 3.29 eV.[69] The band gaps of $P3m1$ and $P2_1/c$ TiOS are smaller than those of the previously reported 2D TiO_2. From the electronic structure it can be seen that the $P3m1$ structure is a direct bandgap semiconductor, with the CBM and the VBM at the G point, whereas the other two structures are indirect bandgap semiconductors with the VBM and CBM not located at the same point.

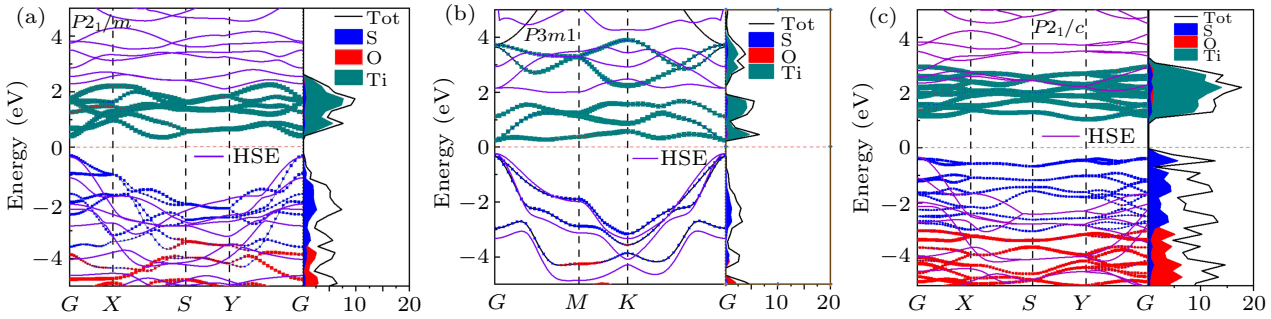


Fig. 6. Energy band structure diagrams and partial density of states of TiOS for (a) $P2_1/m$, (b) $P3m1$ and (c) $P2_1/c$. The energy bands contributed by Ti atoms are shown in green, blue and red show those contributed by S and O atoms, respectively, and purple in the energy band structure diagram shows the energy band calculated with the HSE algorithm.

3.5. Optical properties

It is recognized that 2D semiconductors with band gaps within the range 1.5–3.0 eV exhibit high potential to act as photocatalysts. The band gaps of the three phases are smaller than those of both bulk and 2D TiO_2, so a significant red shift of the absorption edges is expected. In theoretical terms, the capacity of a material to absorb light is connected to its band gap energies. Absorption occurs when the photon energy exceeds the band gap energy, enabling electrons to transition from the valence band to the conduction band, where they can be captured by the material. To investigate the optical absorption properties, we calculated the optical absorption spectrum of the three 2D TiOS structures. As shown in Fig. 7, the absorption spectra of the three TiOS structures cover the entire UV light region, indicating their superior optical absorption. Additionally, pronounced peaks around 400 nm are observed in the visible light region, signifying that these three phases effectively extend their optical absorption range into the visible spectrum.

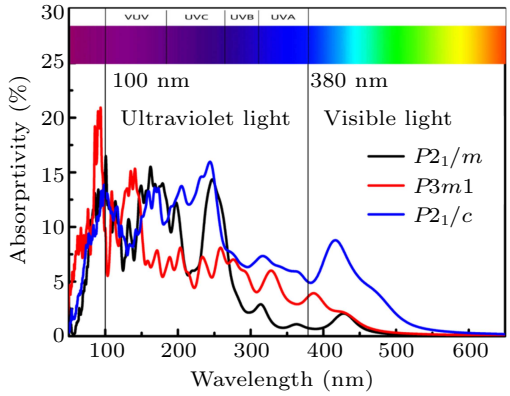


Fig. 7. The optical absorption spectra of the three 2D TiOS structures.

3.6. Photocatalytic properties

Effective photocatalysis for visible-light-driven water decomposition requires a catalyst with both sufficient optical absorption within the visible light range and appropriate band alignments with water. For water, the standard reduction potential of H^+/H_2 and the oxidation potential of O_2/H_2O can be estimated using the following equations:[70]

$$E^{\mathrm{red}}\left(\mathrm{H^+/H_2}\right) = -4.44 + \mathrm{pH} \times 0.059\ \mathrm{eV}, \tag{5}$$

$$E^{\mathrm{OX}}\left(\mathrm{O_2/H_2O}\right) = -5.67 + \mathrm{pH} \times 0.059\ \mathrm{eV}. \tag{6}$$

Typically, the reduction potential of H^+/H_2 and the oxidation potential of O_2/H_2O are calculated for pH = 0 under acidic conditions and pH = 7 under neutral conditions. Different reactions have different redox potentials.

We have performed calculations on the positions of the CBM and VBM using accurate HSE function for three phases, The results of these calculations are shown in Fig. 8. The position of the energy band edges (bottom of the conduction band and top of the valence band) of the material are compared with the redox potential of water. Theoretically, a material is considered to exert a strong driving force for water redox reactions if its band gap encompasses the redox potential.

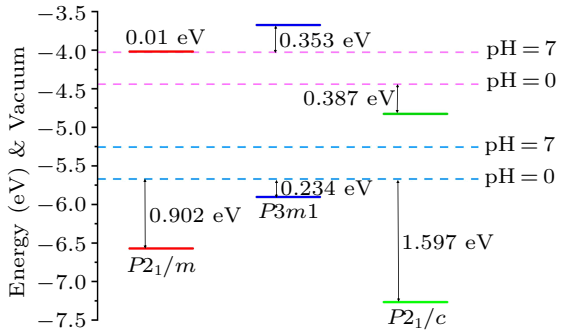


Fig. 8. Comparison of band gap and water redox potential for 2D TiOS structures. The energy is in the vertical coordinate and the different TiOS structures in the horizontal coordinate. The redox potential of water at different pH values is given by the dashed line.

As shown in Fig. 8, the CBMs of 2D $P2_1/m$ and $P3m1$ TiOS materials are higher than the reduction potential of H^+/H_2 at pH = 7, and their VBMs are lower than the oxidation potential of O_2/H_2O at pH = 0, exhibiting good catalytic activity under both acidic and alkaline conditions. For the $P2_1/c$ phase of TiOS, although the VBM is much lower than the oxidation potential of O_2/H_2O at pH = 7, the CBM is lower than the reduction potential H^+/H_2 even at pH = 0, indicating that it might not be a suitable photocatalytic material.

We further investigated the HER performance of the TiOS materials. The Gibbs free energy of H^* (ΔG_{H^*}) was calculated as a key descriptor of hydrogen evolution. Theoretically, the closer the Gibbs free energy is to zero, the better the HER catalytic performance. The calculated ΔG_{H^*} values for the $P2_1/m$ and $P3m1$ TiOS were 1.02 eV and 0.67 eV, respectively. The Janus phase $P3m1$ possesses a smaller ΔG_{H^*} value than that of the $P2_1/m$ phase. Overall, the ΔG_{H^*} values are not close to zero, which is not surprising for the TiOS 2D materials since they are similar to TiO_2. For example, the ΔG_{H^*} values of the hydrogen atoms absorbed on the two-coordinated and three-coordinated O atoms sites for anatase TiO_2 (101 surface) were reported to be 1.76 eV and 1.17 eV, respectively.[71] For TiO_2 nanosheets, ΔG_{H^*} was found to be 3.423 eV.[72] Thus, as a similar system to TiO_2, the 2D TiOS materials also exhibit a relatively large ΔG_{H^*}. Similar to TiO_2, further functionalization and modification of the TiOS 2D materials are required to enhance their photocatalytic properties. Many methods, such as metal and non-metal doping, vacancy introduction and stress engineering, have been shown to be effective in improving photocatalytic performance. Further work to improve the photocatalytic properties of TiOS is ongoing and will be reported later. Overall, we have designed two new TiO_2-like 2D TiOS materials, and found that they have suitable band gaps as well as good potential for photocatalysis.

4. Conclusion

In this paper, to design a more effective photocatalytic material, we identified three two-dimensional semiconductor TiOS materials using swarm intelligence algorithms combined with first-principles calculations. Structurally, the newly discovered 2D TiOS materials retain the overall honeycomb lattice structure characteristic of MoS_2. However, the different arrangement of oxygen and sulfur atoms on either side of the titanium atomic layer results in three different 2D TiOS phases with space groups $P2_1/m$, $P3m1$ and $P2_1/c$, respectively. The structural stabilities of the three 2D TiOS phases were checked by the cohesive energy, phonon curves and elastic constants, and molecular dynamics simulations. Electronic results indicate that the Janus $P3m1$ phase is a direct bandgap semiconductor, while the $P2_1/m$ and $P2_1/c$ phases are indirect bandgap semiconductors. Using the accurate HSE functions, the corresponding band gaps of the three structures were calculated to be 2.34 eV ($P2_1/m$), 2.24 eV ($P3m1$) and 3.22 eV ($P2_1/c$), respectively. Optical property calculations reveal that the TiOS materials exhibit a good light-harvesting capability in both visible and UV spectral ranges. Moreover, we revealed that both $P2_1/m$ and $P3m1$ TiOS can provide a strong driving force for converting H_2O to H_2 and O_2 in an acidic environment with pH = 0. The suitable band gap, moderate absorption and strong driving force for the conversion of H_2O to H_2 and O_2 in acidic conditions suggest that TiOS materials possess good photocatalytic properties, and could serve as potential new photocatalysts.

Acknowledgements

This work was financially supported by the National Natural Science Foundation of China (Grant Nos. 52272219 and U1904612) and the Natural Science Foundation of Henan Province (Grant No. 242300421191).

References

[1] Ma Y, Wang X, Jia Y, Chen X, Han H and Li C 2014 *Chem. Rev.* **114** 9987
[2] A G F 1959 *Rev. Mod. Phys.* **31** 646
[3] Diebold U 2003 *Surf. Sci. Rep.* **48** 53
[4] Diasanayake M, Senadeera G, Sarangika H, Ekanayake P, Thotawattage C, Divarathne H and Kumari J 2016 *Mater. Today: Proc.* **3** S40
[5] Zakir O, Ait-Karra A, Idouhli R, Khadiri M, Dikici B, Aityoub A, Abouelfida A and Outzourhit A 2023 *J. Solid State Electr.* **27** 2289
[6] Pourmadadi M, Rajabzadeh-Khosroshahi M, Eshaghi M M, Rahmani E, Motasadizadeh H, Arshad R, Rahdar A and Pandey S 2023 *J. Drug Deliv. Sci. Tec.* **82** 104370
[7] Ge S, Sang D, Zou L, Yao Y, Zhou C, Fu H, Xi H, Fan J, Meng L and Wang C 2023 *Nanomaterials* **13** 1141
[8] Fujishima A and Honda K 1972 *Nature* **238** 37
[9] Lacerda A M, Larrosa I and Dunn S 2015 *Nanoscale* **7** 12331
[10] Wang J, Guo R T, Bi Z X, Chen X, Hu X and Pan W G 2022 *Nanoscale* **14** 11512
[11] Singh R and Dutta S 2018 *Fuel Cells* **220** 607
[12] Baig U, Uddin M K and Sajid M 2020 *Mater. Today Commun.* **25** 101534
[13] Prakash J, Kumar A, Dai H, Janegitz B C, Krishnan V, Swart H C and Sun S 2021 *Mater. Today Sustain.* **13** 100066
[14] Li Y, Shen Q, Guan R, Xue J, Liu X, Jia H, Xu B and Wu Y 2020 *J. Mater. Chem. C* **8** 1025
[15] Ji J, Liu B, Huang H, Wang X, Yan L, Qu S, Liu X, Jiang H, Duan M and Li Y 2021 *J. Mater. Chem. C* **9** 7057
[16] Wang J, Fu K, Zhang X, Yin Q, Wei G and Su Z 2021 *J. Mater. Chem. C* **9** 8466
[17] Schneider J, Matsuoka M, Takeuchi M, Zhang J, Horiuchi Y, Anpo M and Bahnemann D W 2014 *Chem. Rev.* **114** 9919
[18] Zhang J, Wu Y, Xing M, Leghari S A K and Sajjad S 2010 *Energ. Environ. Sci.* **3** 715
[19] Etghani S A, Ansari E and Mohajerzadeh S 2019 *Sci. Rep.* **9** 17943
[20] Zhong J, Chen F and Zhang J 2010 *J. Phys. Chem. C* **114** 933
[21] Piątkowska A, Janus M, Szymański K and Mozia S 2021 *Catalysts* **11** 144
[22] Umezawa N, Janotti A, Rinke P, Chikyow T and Van de Walle C G 2008 *Appl. Phys. Lett.* **92** 041104
[23] Cui Y, Du H and Wen L 2009 *Solid State Commun.* **149** 634
[24] Umebayashi T, Yamaki T, Itoh H and Asai K 2002 *Appl. Phys. Lett.* **81** 454
[25] Huang Z, Gao Z, Gao S, Wang Q, Wang Z, Huang B and Dai Y 2017 *Chin. J. Catal.* **38** 821
[26] Sharotri N and Sud D 2015 *New J. Chem.* **39** 2217
[27] Bu X, Wang Y, Li J and Zhang C 2015 *J. Alloys Compd.* **628** 20
[28] Lin Y H, Chou S H and Chu H 2014 *J Nanopart Res.* **16** 2539
[29] Kovačić M, Perović K, Papac J, Tomić A, Matoh L, Žener B, Brodar T, Capan I, Surca A K and Kušić H 2020 *J. Materials* **13** 1621
[30] Ramanathan R and Bansal V 2015 *J. RSC Advances* **5** 1424
[31] El Nemr A, Helmy E T, Gomaa E A, Eldafrawy S and Mousa M 2019 *J. Environ. Chem. Eng.* **7** 103385
[32] Shvadchina Y O, Cherepivskaya M, Vakulenko V, Sova A, Stolyarova I and Prikhodko R 2015 *J. Water Chem. Technol.* **37** 283
[33] Kang I C, Zhang Q, Yin S, Sato T and Saito F 2008 *Environ. Sci. Technol.* **42** 3622
[34] Jovanovic D, Zagorac D, Matovic B, Zarubica A and Zagorac J 2021 *Acta Crystallogr. Sect. B: Struct. Sci.* **77** 833
[35] Xiang Y J, Gao S, Wang C, Fang H, Duan X, Zheng Y F and Zhang Y Y 2024 *Chin. Phys. B* **33** 087101
[36] Barhoumi M, Said I, Yedukondalu N and Said M 2023 *Results Phys.* **48** 106438
[37] Wang Y, Lv J, Zhu L and Ma Y 2012 *Comput. Phys. Commun.* **183** 2063
[38] Kresse G and Hafner J 1994 *Phys. Rev. B* **49** 14251
[39] Kresse G and Furthmüller J 1996 *Comput. Mater. Sci.* **6** 15
[40] Kresse G and Furthmüller J 1996 *Phys. Rev. B* **54** 11169
[41] Perdew J P, Burke K and Ernzerhof M 1996 *Phys. Rev. Lett.* **77** 3865
[42] Kresse G and Joubert D 1999 *Phys. Rev. B* **59** 1758
[43] Monkhorst H J and Pack J D 1976 *Phys. Rev. B* **13** 5188
[44] Heyd J, Scuseria G E and Ernzerhof M 2003 *J. Chem. Phys.* **118** 8207
[45] Yuan J H, Song Y Q, Chen Q, Xue K H and Miao X S 2019 *Appl. Surf. Sci.* **469** 456
[46] Togo A and Tanaka I 2015 *Scr. Mater.* **108** 1
[47] Dudarev S L, Botton G A, Savrasov S Y, Humphreys C and Sutton A P 1998 *Phys. Rev. B* **57** 1505
[48] Zhang L, Yang Z, Gong T, Pan R, Wang H, Guo Z, Zhang H and Fu X 2020 *J. Mater. Chem. A* **8** 8813
[49] Zheng T, Lin Y C, Yu Y, Valencia-Acuna P, Puretzky A A, Torsi R, Liu C, Ivanov I N, Duscher G and Geohegan D B 2021 *Nano Lett.* **21** 931
[50] Lu A Y, Zhu H, Xiao J, Chuu C P, Han Y, Chiu M H, Cheng C C, Yang C W, Wei K H and Yang Y 2017 *Nat. Nanotechnol.* **12** 744
[51] Zhou W, Chen J, Yang Z, Liu J and Ouyang F 2019 *Phys. Rev. B* **99** 075160
[52] Peng R, Ma Y, Huang B and Dai Y 2019 *J. Mater. Chem. A* **7** 603
[53] Li L, Yang Z X, Huang T, Wan H, Chen W Y, Zhang T, Huang G F, Hu W and Huang W Q 2024 *Appl. Phys. Lett.* **125** 223904
[54] Frey N C, Bandyopadhyay A, Kumar H, Anasori B, Gogotsi Y and Shenoy V B 2019 *J. ACS Nano* **13** 2831
[55] Abdollahi M and Tagani M B 2022 *J. Phys. Condens. Matter* **34** 185702
[56] Zhang C, Nie Y, Sanvito S and Du A 2019 *Nano Lett.* **19** 1366
[57] Koo H C, Kim S B, Kim H, Park T E, Choi J W, Kim K W, Go G, Oh J H, Lee D K and Park E S 2020 *Adv. Mater.* **32** 2002117

[58] Bihlmayer G, Rader O and Winkler R 2015 *New J. Phys.* **17** 050202
[59] Ahmad S and Mukherjee S 2014 *J. Graphene* **3** 52
[60] Yang L M, Bacic V, Popov I A, Boldyrev A I, Heine T, Frauenheim T and Ganz E 2015 *J. Am. Chem. Soc.* **137** 2757
[61] Guan J, Zhu Z and Tománek D 2014 *Phys. Rev. Lett.* **113** 046804
[62] Mouhat F and Coudert F X 2014 *Phys. Rev. B* **90** 224104
[63] Tang W, Sanville E and Henkelman G 2009 *J. Phys. Condens. Matter* **21** 084204
[64] Nye J F 1985 *Physical properties of crystals: their representation by tensors and matrices* (2nd edn.) (Oxford: Clarendon Press) pp. 182–184
[65] Peng R, Ma Y, He Z, Huang B, Kou L and Dai Y 2019 *Nano Lett.* **19** 1227
[66] Li P, You Z, Haugstad G and Cui T 2011 *Appl. Phys. Lett.* **98** 253105
[67] Li P 2019 *Phys. Chem. Chem. Phys.* **21** 11150
[68] Liu F, Ming P and Li J 2007 *Phys. Rev. B* **76** 064120
[69] Xiong Z Q, Zhang P C, Kang W B and Fang W Y 2020 *Acta Phys. Sin.* **69** 166301 (in Chinese)
[70] Chen S and Wang L W 2012 *Chem. Mater.* **24** 3659
[71] Yang N, Zhao Y, He T, Wang K, Luo Z, Zheng H, Shen Y, Santiago A R P, Zhou T and Zhan W 2024 *ACS Appl. Nano Mater.* **7** 9598
[72] Wu X, Zuo S, Qiu M, Li Y, Zhang Y, An P, Zhang J, Zhang H and Zhang J 2021 *Chem. Eng. J.* **420** 127681